1760 *Chem. Mater.* **2010,** *22,* 1760–1767
DOI:10.1021/cm903207q

CHEMISTRY OF MATERIALS
Article

Direct Synthesis of Controllable Microstructures of Thermally Stable and Ordered Mesoporous Crystalline Titanium Oxides and Carbide/Carbon Composites

Chun-Hsien Huang,[†] Dong Gu,[‡] Dongyuan Zhao,[‡] and Ruey-An Doong*,[†]

[†]*Department of Biomedical Engineering and Environmental Sciences, National Tsing-Hua University, Hsinchu, 30013, Taiwan, and* [‡]*Department of Chemistry, Shanghai Key Laboratory of Molecular Catalysis and Innovative Materials and Advanced Materials Laboratory, Fudan University, Shanghai, 200433, P. R. China*

Received October 17, 2009. Revised Manuscript Received January 15, 2010

The mesoporous titanium oxides- and carbide-carbon nanocomposites (Ti−C nanocomposites) with different morphologies at various Ti/C mass ratios were directly synthesized via supramolecular self-assembly with in situ crystallization process. The microstructures including surface area, morphology, and crystallinity were characterized by surface area analyzer, TEM, and SAXS/XRD, respectively. The specific BET surface areas (178−639 $m^2\ g^{-1}$), micropore surface areas (6.3−47.3%), and total pore volumes (0.18−0.46 $cm^3\ g^{-1}$) increase with the increase in calcination temperatures and Ti/C mass ratios. The calcination temperature and carbon content have significant effect on the thermal stability of titanium-based nanomaterials. The crystallinity changes from anatase, rutile, Magneli phases, and then to TiC when the carbon content is lower than 35 wt %, while the crystal phase of Ti−C composites at 50 wt % changes directly from anatase to TiC. However, Mageli products lose the mesostructures. The sizes of TiO_2 nanocrystals are in the range 2.6−9.7 nm, and increase with increasing temperature to slightly distort the ordered mesostructured regularity up to 800 °C, and low distorted octahedrons with 6-fold coordinated titanium carbide are formed at 1000 °C. In addition, the graphitized carbons, determined by sp^2- and sp^3-bonded carbon contents from XAS spectra, increased upon increasing calcination temperature, depicting the increase in graphitization after calcination. Results obtained in this study allow us to elucidate the microstructural changes of titanium-based materials inside the highly ordered mesoporous carbon matrices and open an avenue to the design and synthesis of a multitude of cooperatively functional organic−inorganic materials with attractive novel properties.

Introduction

Ordered mesoporous materials (OMMs) including ordered mesoporous carbons (OMCs), metal oxides, and nonoxides having large surface areas, controllable pore sizes, high adsorption capacity, and large pore volumes, have recently become attractive for a wide variety of potential applications in fields of adsorption, purification, catalysis, gas storage, sensing devices, energy storage, and conversion.[1−6] In general, OMMs can be prepared by hard and soft templating synthetic methods.[1] The hard templating approach impregnates periodically ordered structure matrices, such as ordered mesoporous silica (SBA-15 and MCM-41), with organic and inorganic precursors to design the framework, mesostructures, and surface chemistry of OMMs. Although the hard-templating method has advantages of simplicity and fidelity in producing the ordered nanostructures, the procedure is usually quite long and tedious because several steps are required to fabricate the structure matrices and then remove the siliceous template matrices under harsh chemical treatment conditions.

The soft templating process generates the carbon nanostructures through self-assembly of amphiphilic molecules. The polystyrene-*b*-poly(4-vinylpyridine)/resorcinol-formaldehyde system was used to synthesize the OMCs.[1b]

*Corresponding author. 101, sec. 2, Kuang-Fu Rd., Department of Biomedical Engineering and Environmental Sciences, National Tsing-Hua University, Hsinchu, 30013, Taiwan. E-mail: radoong@mx.nthu.edu.tw. Phone: +886-3-5726785. Fax: +886-3-5718649.

(1) (a) Liang, C. D.; Li, Z. J.; Dai, S. *Angew. Chem., Int. Ed.* **2008**, *47*, 3696–3717. (b) Liang, C. D.; Hong, K.; Guiochon, G. A.; Mays, J. M.; Dai, S. *Angew. Chem., Int. Ed.* **2004**, *43*, 5785–5789. (c) Jun, S.; Joo, S. H.; Ryoo, R.; Kruk, M.; Jaroniec, M.; Liu, Z.; Ohsuna, T.; Terasaki, O. *J. Am. Chem. Soc.* **2000**, *122*, 10712–10713. (d) Jun, Y.; Hong, H.; Antonietti, M.; Thomas, A. *Adv. Mater.* **2009**, *21*, No. 10.1002/adma.200803500. (e) Tiemann, M. *Chem. Mater.* **2008**, *20*, 961–971. (f) Yue, W. B.; Xu, X. X.; Irvine, J. T. S.; Attidekou, P. S.; Liu, C.; He, H. Y.; Zhao, D. Y.; Zhou, W. Z. *Chem. Mater.* **2009**, *21*, 2540–2546. (g) Yue, W. B.; Randorn, C.; Attidekou, P. S.; Su, Z. X.; Irvine, J. T. S.; Zhou, W. Z. *Adv. Funct. Mater.* **2009**, *19*, 2826–2833.
(2) Hagfeldt, A.; Grätzel, M. *Chem. Rev.* **1995**, *95*, 49–68.
(3) Topoglidis, E.; Cass, A. E. G.; Gilardi, G.; Sadeghi, S.; Beaumont, N.; Durrant, J. R. *Anal. Chem.* **1998**, *70*, 5111–5113.
(4) Roggenbuck, J.; Tiemann, M. *J. Am. Chem. Soc.* **2005**, *127*, 1096–1097.
(5) Meng, Y.; Gu, D.; Zhang, F. Q.; Shi, Y. F.; Yang, H. F.; Li, Z.; Yu, C. Z.; Tu, B.; Zhao, D. Y. *Angew. Chem., Int. Ed.* **2005**, *44*, 7053–7059.
(6) Zhang, F.; Gu, D.; Yu, T.; Zhang, F.; Xie, S.; Zhang, L.; Deng, Y.; Wan, Y.; Tu, B.; Zhao, D. *J. Am. Chem. Soc.* **2007**, *129*, 7746–7747.

Published on Web 01/29/2010

More recently, the triblock copolymers have been successfully employed as a structure-directing agent (SDA) for the preparation of OMC via organic−organic assembly of amphiphilic copolymers and phenolic resins.[5,6] In addition, multifunctional mesoporous carbon-based materials are also of great significance in a wide variety of applications because of the merits from synergistic roles of each component.[2,7] Recently, the ordered mesoporous carbon−silica nanocomposites can be synthesized via the sol−gel process and supramolecular self-assembly approach by addition of silicates into frameworks to enhance the toughness of carbons and resist the thermal shrinkage.[8]

Titanium-based materials, such as anatase, rutile, Magneli phases, and titanium carbide (TiC), are one of the most interesting nanostructures for a wide variety of applications because of their unique photoinduced electron transfer, high chemical stability, high hardness and corrosion resistance, nontoxicity, and electrical conductivity.[2,9−12] Increasing attention has been attempted to simultaneously achieve high crystallinity and mesostructural regularity of TiO_2 frameworks with high thermal stability. The combination of advantages of both soft- and hard-templating approaches and the utilization of reinforcement (carbon or SiO_2) to control the mesoporosity during the high temperature crystallization of the metal oxide composites has recently been studied.[12] Because of the novel physicochemical properties and multifunctionality, the combination of carbon- and titanium-based materials has immense potential for a wide variety of applications. The synthesis of the mesoporous carbon−titania nanocomposites has the advantages of coupling the photoactivity of anatase with the adsorptive capacity of carbon for effective photocatalytic degradation of Rhodamine B and methylene blue.[11a,b] The ordered mesoporous carbon−titanium materials also good electrical conductivity and high surface areas, which enable the application to lithium-ion battery because of the improved electrical property, ionic transport, and rate capability.[11d] In addition, an ordered mesoporous nanocrystalline TiC/carbon composite was fabricated by using a solvent-evaporation-induced self-assembly (EISA) approach combined with in situ carbothermal reduction.[10] However, the fabrication of titanium-based nanostructures with different morphologies including anatase, rutile, Magneli phases, and TiC in the presence of ordered mesoporous carbon materials from in situ carbothermal reduction methods has rarely reported. In addition, the effect of carbon contents and calcination temperatures on the microstructures of titanium-based materials remains unclear. It is therefore highly important to design and construct the phase evolution of titania and degree of graphitization of carbon in titanium oxides and carbide/carbon (Ti−C) composites.

Herein, we report a facile route to directly synthesize mesoporous Ti−C composites with different morphologies at various Ti/C mass ratios via supramolecular self-assembly with in situ crystallization process. The soluble resol polymer, prehydrolyzed $TiCl_4$, and triblock copolymer F127 were employed as a carbon precursor, an inorganic precursor, and a SDA, respectively, to fabricate the controllable properties of mesoporous titanium−carbon composites. The nanocomposites were characterized with SAXS, XRD, TEM, surface area analyzer, and TGA/DTA to investigate the change in microstructures of titanium-based materials inside the highly ordered mesoporous carbon matrices. In addition, the change in graphitized carbons is determined by X-ray absorption spectroscopy (XAS). We have shown that crystalline phases of titanium-based nanocrystals, taking advantages of the properties of both carbon and TiO_2, can be controlled by calcination temperatures and carbon mass loadings. The ordered mesoporous Ti−C composites with numerous physicochemical properties and interconnected pore structures would benefit their practical applications, such as electrodes for lithium-ion batteries and adsorbents and photocatalyst for environmental purification.

Experimental Section

Chemicals. Titanium tetrachloride ($TiCl_4$) and amphiphilic triblock copolymer Pluronic F127 ($OH(CH_2CH_2O)_n-(CH_2CH(CH_3)O)_m-(CH_2CH_2O)_nH$, $EO_{106}PO_{70}EO_{106}$) were obtained from Acros Corp. Phenol, formalin solution (37 wt % formaldehyde), and anhydrous ethanol were purchased from Shanghai Chemical Corp. All other chemicals were of analytical grade and used as received without further purification. All solutions were prepared using bidistilled deionized water (Millipore, 18.3 MΩ cm) unless otherwise mentioned.

Synthesis of Titanium Oxide and Carbide/Carbon Composites. The supramolecular self-assembly methods followed by in situ crystallization technology was employed to prepare titanium oxides and carbide/carbon composites. A 20 wt % resol ethanolic solution was first synthesized according to an established method.[5] A 20 wt % prehydrolyzed $TiCl_4$ solution was first prepared by dropping $TiCl_4$ into the mixture containing ethanol and deionized water (50:50 w/w) at room temperature under vigorous stirring conditions for 30 min. In a typical synthesis of the 65Ti-35C composite, 1.5 g of triblock copolymer F127 was dissolved in 10.0 g of anhydrous ethanol. Then, 1.1 g of 20 wt % resol ethanolic solution and 7.4 g of 20 wt % prehydrolyzed $TiCl_4$ solution were added slowly with stirring for 1 h at room temperature. The homogeneous mixture was then transferred into the Petri dishes at 40 °C for 24 h in an oven. After being

(7) Wan, Y.; Shi, Y. F.; Zhao, D. Y. *Chem. Mater*. **2008**, *20*, 932–945.
(8) Liu, R. L.; Shi, Y. F.; Wan, Y.; Meng, Y.; Zhang, F. Q.; Gu, D.; Chen, Z. X.; Tu, B.; Zhao, D. Y. *J. Am. Chem. Soc*. **2006**, *128*, 11652–11662.
(9) (a) Toyoda, M.; Yano, T.; Tryba, B.; Mozia, S.; Tsumura, T.; Inagaki, M. *Appl. Catal., B* **2009**, *88*, 160–164. (b) Jiang, Z.; Rhine, W. E. *Chem. Mater*. **1991**, *3*, 1132–1137. (c) Shin, Y.; Li, X. S.; Wang, C.; Coleman, J. R.; Exarhos, G. J. *Adv. Mater*. **2004**, *16*, 1212–1215.
(10) Yu, T.; Deng, Y.; Wang, L.; Liu, R. L.; Zhang, L.; Tu, B.; Zhao, D. Y. *Adv. Mater*. **2007**, *19*, 2301–2306.
(11) (a) Liu, R. L.; Ren, Y. J.; Shi, Y. F.; Zhang, F.; Zhang, L. J.; Tu, B.; Zhao, D. Y. *Chem. Mater*. **2008**, *20*, 1140–1146. (b) Hsu, Y. C.; Lin, H. C.; Lue, C. W.; Liao, Y. T.; Yang, C. M. *Appl. Catal., B* **2009**, *89*, 309–314. (c) Stefik, M.; Lee, J.; Wiesner, U. *Chem. Commun*. **2009**, 2532–2534. (d) Guo, Y. G.; Hu, J. S.; Wan, L. J. *Adv. Mater*. **2008**, *20*, 2878–2887.
(12) (a) Kondo, J. N.; Domen, K. *Chem. Mater*. **2008**, *20*, 835–847. (b) Lee, J.; Orilall, M. C.; Warren, S. C.; Kamperman, M.; Disalvo, F. J.; Wiesner, U. *Nat. Mater*. **2008**, *7*, 222–228.

Table 1. Physicochemical Characterization of the Titanium Oxides and Carbide/Carbon (Ti−C) Composites

sample[a]	unit cell parameter[b] (nm)	pore size[c] (nm)	surface area ($m^2\ g^{-1}$)	pore volume ($cm^3\ g^{-1}$)	micropore surface area ($m^2\ g^{-1}$)	d[d] (nm)	crystal phase[e] (nm)
75Ti-25C as-made	16.8						
75Ti-25C-450	11	4.4	178	0.18	17	4.7	A
75Ti-25C-600	11	3.8	307	0.22	39	6.8	A
75Ti-25C-700	11	3.8	329	0.23	35	7.5	A
75Ti-25C-800	[f]	3.9	377	0.26	54	9.7	A 57%, R 43%
75Ti-25C-1000		3.8	347	0.36	22	12.1(TiC)	TiC + Ti_4O_7
65Ti-35C as-made	16.3						
65Ti-35C-450	10.7	5.4	285	0.29	47	2.6	A
65Ti-35C-600	10.7	3.8	376	0.25	89	6.5	A
65Ti-35C-700	10.7	4.8	449	0.33	113	8.1	A
65Ti-35C-800	10.7	4.3	512	0.34	106	9.4	A 78%, R 22%
65Ti-35C-1000		3.9	486	0.43	58	10.1(TiC)	TiC + Ti_4O_7
50Ti-50C as-made	15.6						
50Ti-50C-450	10.8	4.9	365	0.34	75		
50Ti-50C-600	10.8	4.8	434	0.36	172		
50Ti-50C-700	10.7	4.9	489	0.41	203		
50Ti-50C-800	10.7	4.9	556	0.42	262	4.2	A
50Ti-50C-1000	10.4	4.9	639	0.46	302	4.6(TiC)	TiC

[a] (100-*m*)Ti-*m*C-*x*, where *x* and *m* represent the calcination temperature and weight percentage of carbon content in composites, respectively. [b] The unit-cell parameter is calculated by the formula $a_o = 2/d_{10}\sqrt{3}$. [c] Pore size diameter is calculated by the BJH method from adsorption data of N_2 isotherms. [d] The nanocrystallite size of anatase is calculated by Scherrer formula using the full-width half-maximum of the 101 peak. [e] The weight percentage of anatase (A) and rutile (R) is calculated by the formula: content of anatase (%) = $I_A/(I_A + 1.265I_R) \times 100$, where I_A and I_R are main peak intensities of anatase and rutile, respectively. [f] not determined.

dried, the films were heated at 100 °C for another 24 h. The as-made products, the orange transparent membranes, were scraped from the Petri dishes and ground into powders. Calcination was carried out in a tubular furnace at various temperatures ranging from 450 to 1000 °C under a N_2 atmosphere at a flow rate of 100 mL/min. The heating programs started from ambient temperature to the desired temperature (450−1000 °C) at a rate of 1 °C/min, held for 3 h at 450−600 °C or for 0 h at 800−1000 °C, and then cooled to room temperature. The titanium oxide and carbide/carbon composites, denoted as (100-*m*)Ti-*m*C-*x* (where *x* and *m* represent the calcination temperature and weight percentage of carbon in the materials, respectively), were fabricated and characterized.

Characterization and Measurement. The small-angle X-ray scattering (SAXS) measurements were taken on a Nanostar U small-angle X-ray scattering system (Bruker, Germany) using Cu Kα radiation (40 kV, 35 mA). The *d*-spacing and unit cell parameters were calculated by the formula $d = 2\pi/q$ and $a_0 = 2d_{10}/\sqrt{3}$, respectively. Transmission electron microscopy (TEM) images were collected using a JEOL 2011 microscope (200 kV). The samples were suspended in ethanol. Wide-angle XRD patterns were recorded on a Bruker D4 X-ray diffractometer with Ni-filtered Cu Kα radiation (40 kV, 40 mA). The crystallite size was estimated by applying the Scherrer equation to the fwhm of the 101 peak of anatase.

$$\mathrm{d} = \frac{0.89\lambda}{B\theta_B} \tag{1}$$

where *d* is the crystal size, *B* the full-width at half-maximum (fwhm), λ the wavelength of Cu Kα-irradiation source, and θ_B a Bragg angle of $2\theta/2$.

The X-ray adsorption near-edge structure (XANES) spectra of C and Ti *K*-edge in Ti−C composites were measured in total X-ray fluorescence yield mode at room temperature using BL-20A and BL-16A, respectively, at National Synchrotron Radiation Research Center (NSRRC, Hsinchu, Taiwan) in which the electron storage ring was operated at 1.5 GeV with a beam current of 300 mA. For beamline 20A, samples were ground to powder, then secured onto conducting tape, and subjected to an ultrahigh vacuum chamber (1×10^{-9} Torr). For C *K*-edge absorption, the data were collected at the 6 m high energy spherical grating monochromator (HSGM) beamline with 10×10 μm opening slits, corresponding to ~0.08 eV energy resolution. Simultaneously, the signal from a gold grid located upstream in the X-ray path was recorded, and the spectra were normalized using the incident beam intensity, I_0, keeping the area under the spectra fixed over an energy range of 316 and 325 eV for the C *K*-edge. For beamline 16A, the Ti *K*-edge absorption spectra were measured in fluorescence yield mode using a Lytle detector with powder sample dispersed onto Kapton tape. X-rays were monochromated by using a Si(111) double monochromator before reflecting off a higher-order harmonic light rejection mirror. The energy scale was calibrated using the L_3-edge of a Mo foil at 2520 eV. Energy steps as small as 0.2 eV were employed near the absorption edges with a accounting time of 2 s per step.

Nitrogen adsorption−desorption isotherms were collected at 77 K using Micromeritics Tristar-3020 and Micromeritics 2020 analyzer (USA). The Brunauer−Emmett−Teller (BET) method was utilized to calculate the specific surface areas (S_{BET}) using adsorption data in a relative pressure range from 0.02 to 0.2. Using the Barrett−Joyner−Halenda (BJH) model, the pore volumes and pore size distributions in the mesopore range (>2 nm) were derived from the adsorption branches of the isotherms, and the total pore volumes (V_t) were estimated from the adsorbed amount at a relative pressure P/P_0 of 0.995. Using the Horvath−Kawazoe (HK) model, the micropore distribution (<2 nm) were derived from the adsorption branches of the isotherms in a relative pressure range from 1×10^{-7} to 1×10^{-2}. The micropore surface areas (S_{mi}) were calculated from the *t*-plot method. The *t* values were calculated as a function of the relative pressure (P/P_0) ranging from 0.08 to 0.30 using the de Bore equation, t (Å) = $[13.99/(\log(p_0/p) + 0.0340)]^{1/2}$, which correspond to the *t* values of 0.35−0.5 nm. Weight changes of the products were carried out on a Mettler Toledo TGA/SDTA851 analyzer (Switzerland) from 50 to 1200 °C under nitrogen or air at a heating rate of 30 °C/min. Raman spectra were obtained with a micro-Raman spectrophotometer, using monochromatic radiation emitted by a Ar laser (488 nm).

Results and Discussion

Table 1 shows the detailed microstructures of (100-*m*)Ti-*m*C nanocomposites calcined at various temperatures under anoxic conditions. To confirm the carbon content of each nanocomposites, the Ti−C materials were first heated to 600 °C under anoxic conditions to remove surfactants and carbonize the resol polymers. The weight percentage of carbon content in Ti−C composites was then determined by TGA in air from room temperature to 800 °C. The determined weight percentages of carbon content are 27, 37, and 54% for 75Ti-25C, 65Ti-35C, and 50Ti-50C composites, respectively, which are in good agreement with the theoretical values (see Figure S1 in the Supporting Information). The distribution of pore diameters of the mesoporous composites, calculated from the adsorption branch of N_2 isotherms based on the BJH model, is narrow (see Figures S2−S4 in the Supporting Information). With the increase in the calcination temperatures and C/Ti mass ratios, the specific BET surface areas (178−639 $m^2\ g^{-1}$), micropore surface areas (6.3−47.3%) derived from the *t*-plots, and total pore volumes (0.18−0.46 $cm^3\ g^{-1}$) increase gradually. With the increase in calcination temperatures, the pore sizes of 75Ti-25C and 65Ti-35C composites decrease, whereas those of 50Ti-50C composite are unchanged, indicating that the 50Ti-50C composite has a higher thermal stability, which is in good agreement with SAXS results (see Figure S5 in the Supporting Information). In addition, the oxidation of carbon phase and structural reorganization during pyrolysis and in situ crystallization processes at 1000 °C generates plenty of micropores in the framework, and results in the increase in the surface area and pore volume of the composites (see Figure S6 in the Supporting Information).

The mesoporous 65Ti-35C composite was chosen to demonstrate the generality of the sample characteristics. Figure 1 shows the SAXS and wide-angle XRD patterns of the composite after being calcined at various temperatures under a N_2 atmosphere. The SAXS pattern of as-made mesoporous 65Ti-35C composite exhibits three scattering peaks which can be indexed as the 10, 11, and 20 reflections, demonstrating the highly ordered 2-D hexagonal mesostructure (*p6mm*) with a unit-cell parameter (a_0) of about 16.3 nm.[11] After calcination at 450 °C, the product turns in black color and its SAXS peaks become broadening (Figure 1a). The 10 scattering peak is still well-resolved, reflecting that the 2D hexagonal mesostructure is retained. It is also noted that the 10 scattering peak shifts to a higher *q* value, depicting the decrease in unit-cell parameter and shrinkage in framework. It is attributed primarily to the degradation of the mesostructure along with the copolymer template decomposition and the crystallization of titania. After being calcined at temperatures higher than 600 °C, the SAXS patterns become poorly resolved and the intensities of the 10 scattering peak decrease significantly, indicating the reduction and distortion of the mesostructured regularity, which may result from the growth and crystallization of the anatase nanocrystals.

Wide-angle XRD patterns (Figure 1b) of the mesoporous 65Ti-35C composites after calcination at various temperatures show that the crystallization of anatase nanocrystals occurs at 450 °C. The diffraction intensities enhance significantly upon the increase in calcination temperature, suggesting an increase in crystallinity. The sizes of anatase nanocrystals, calculated from the Scherrer equation, are in the range 2.6−9.7 nm. No rutile phase, however, is detected on the basis of wide-angle XRD measurements of the mesoporous 65Ti-35C composite when calcination temperature is below 700 °C. In general, the transformation of anatase to rutile TiO_2 occurs at around 600 °C and changes into a single phase of rutile around 800−900 °C.[13] This observation depicts that the temperature for TiO_2 phase transition from anatase to rutile increases in the presence of carbon.[11,13−16]

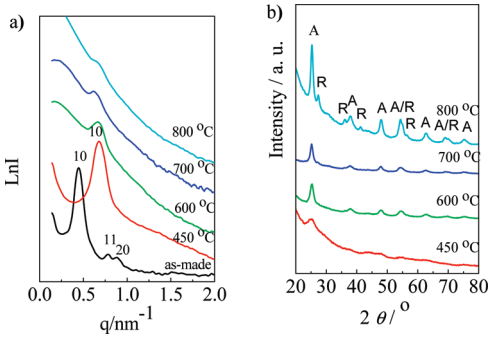

Figure 1. (a) SAXS patterns and (b) wide-angle XRD patterns of the as-made and calcined mesoporous 65Ti-35C composites. The calcination was carried out at various temperatures from 450 to 800 °C under a N_2 atmosphere.

The carbon content is an important factor controlling the mesostructures in the Ti−C composites. SAXS patterns show that all the as-made mesoporous Ti−C composites exhibit three resolved scattering peaks of 2D hexagonal mesostructure (see Figure S5 in the Supporting Information). After being calcined at 450 °C, the peaks can still be observed, which clearly indicate a thermal stability of the mesostructure. The relative contraction is calculated to be in the range 30−34% (Figure 2). In addition, wide angle XRD patterns (see Figure S7 in the Supporting Information) show that the ratio of anatase to rutile at 800 °C increases with the increase in the carbon contents, suggesting that the existence of carbon can stabilize anatase phase (Table 1). The glasslike carbon works as a binder to glue the TiO_2 nanocrystals in the mesoporous Ti−C composites and as an inhibitor for calcination and grain growth of TiO_2 nanocrystals.[13−16] Obviously, the nanocrystalline size of TiO_2 is small and the anatase phase is retained upon increasing the carbon content to 50 wt %. It is reasonable that carbon causes the suppression of phase transition from anatase to rutile and grain growth of nanocrystals.[13]

(13) (a) Inagakia, M.; Hirosea, Y.; Matsunagaa, T.; Tsumurab, T.; Toyoda, M. *Carbon* **2003**, *41*, 2619–2624. (b) Tseng, Y. H.; Lin, H. Y.; Kuo, C. S.; Li, Y. Y.; Huang, C. P. *React. Kinet. Catal. Lett.* **2006**, *89*, 63–69.
(14) Chang, S. M.; Doong, R. A. *J. Phys. Chem. B.* **2006**, *110*, 20808–20814.
(15) (a) LeDuc, C. A.; Campbell, J. M.; Rossin, J. A. *Ind. Eng. Chem. Res.* **1996**, *35*, 2473–2476. (b) Zhang, L. W.; Fu, H. B.; Zhu, Y. F. *Adv. Funct. Mater.* **2008**, *18*, 2180–2189.
(16) Tsumura, T.; Kojitani, N.; Izumi, I.; Iwashita, N.; Toyoda, M.; Inagaki, M. *J. Mater. Chem.* **2002**, *12*, 1391–1396.

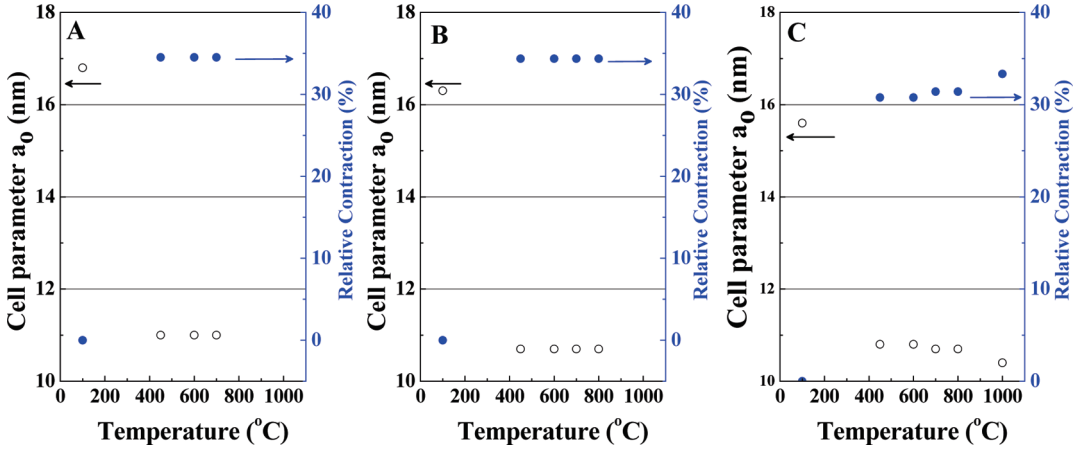

Figure 2. Cell parameters (open circles) and relative contractions (closed circle) of the as-made and calcined mesoporous (A) 75Ti-25C, (B) 65Ti-35C, and (C) 50Ti-50C composites. The calcination was carried out at various temperatures ranging from 450 to 1000 °C in N_2. The calculated relative contraction was determined by the equation of $(a_0'-a_0)/a_0'$, where a_0' and a_0 are cell parameters (a_0) of the as-made and calcined materials, respectively.

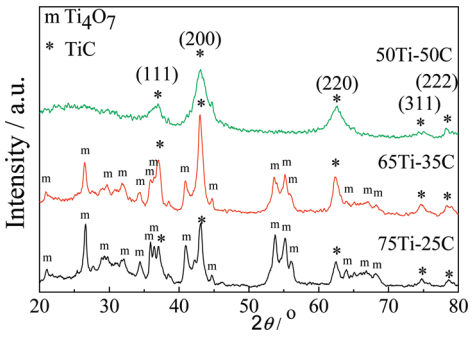

Figure 3. Wide-angle XRD patterns of the mesoporous Ti−C composites at different Ti/C ratios calcined at 1000 °C under a N_2 atmosphere.

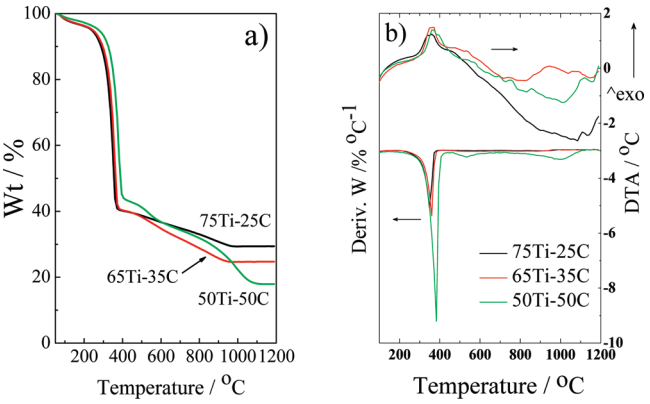

Figure 4. (a) TGA and (b) DTG/DTA curves of as-made mesoporous 75Ti-25C (black line), 65Ti-35C (red line), and 50Ti-50C (green line) composites under a N_2 atmosphere.

A new titania phase is observed after calcined at 1000 °C. Five resolved diffraction peaks at 2θ of 36.8, 42.8, 62.4, 74.9, and 78.4° are observed in the wide-angle XRD patterns (Figure 3), which can be indexed as the (111), (200), (220), (311), and (222) reflections of the cubic TiC nanocrystals with trace amount of oxygen (JCPDS 89−3828). The formation of TiC is mainly attributed to the occurrence of carbothermal reduction reaction ($TiO_2 + 3C \rightarrow TiC + 2CO(g)$) during the pyrolysis.[9,10,17] The carbothermal reduction reaction is usually highly endothermic and proceeds above 1250 °C.[17] In this study, the ordered mesoporous TiC composites were obtained via the sol−gel process, supramolecular self-assembly, and carbothermal reduction reaction. The better homogeneity of TiO_2 nanoparticles with carbon and the high specific surface energy would result in the decrease in the formation temperature of TiC to 1000 °C. The crystalline sizes range between 4.6 and 12.1 nm, and decrease upon increasing the carbon content. In addition, several small diffractions, which can be assigned as Ti_4O_7 phase and unidentified phases (possibly one of Magneli phases), are observed when the carbon content is lower than 35 wt %.

The Ti_4O_7 phase (JCPDS 71−0574) has been known to be one of the Magneli phases, Ti_nO_{2n-1} ($4 \le n \le 9$), with a number of oxygen-defective structures in titania. The crystal structure of Ti_4O_7 is closely related to 2D slabs of rutile separated by a shear plane[18] and can be obtained from the reduction of TiO_2 in ultrahigh vacuum or by carbothermal reduction of ultrafine titania/carbon mixture in controlled atmospheres at high temperature.[9,17−19] Experimentally, the carbon content greatly influences the reaction sequence and crystallization of Magneli phases and TiC during carbothermal reduction reaction. The diffraction intensity for the Ti_4O_7 phase decreases as the carbon content increases from 25 to 50 wt %, whereas only cubic TiC nanocrystals are observed for the mesoporous 50Ti-50C composite at 1000 °C, indicating that the excess carbon led to the formation of TiC at high temperature. This result further confirms that the carbon content significantly influences the reaction sequence, crystallinity and thermal stability of titanium-based nanomaterials. The composited carbon stabilizes the anatase TiO_2 up to 700 °C and transforms to rutile at

(17) (a) Koc, R. *J. Mater. Sci.* **1998**, *33*, 1049–1055. (b) Afir, A.; Achour, M.; Saoula, N. *J. Alloys Compd.* **1999**, *288*, 124–140. (c) Peelamedu, R. D.; Fleming, M.; Agrawal, D. K.; Roy, R. *J. Am. Ceram. Soc.* **2002**, *85*, 117–122.

(18) Abbate, M.; Potze, R.; Sawatzky, G. A.; Schlenker, C.; Lin, H. J.; Tjeng, L. H.; Chen, C. T.; Teehan, D.; Turner, T. S. *Phys. Rev. B* **1995**, *51*, 10150–10153.

(19) Liborio, L.; Harrison, N. *Phys. Rev. B* **2008**, *77*, 104104.

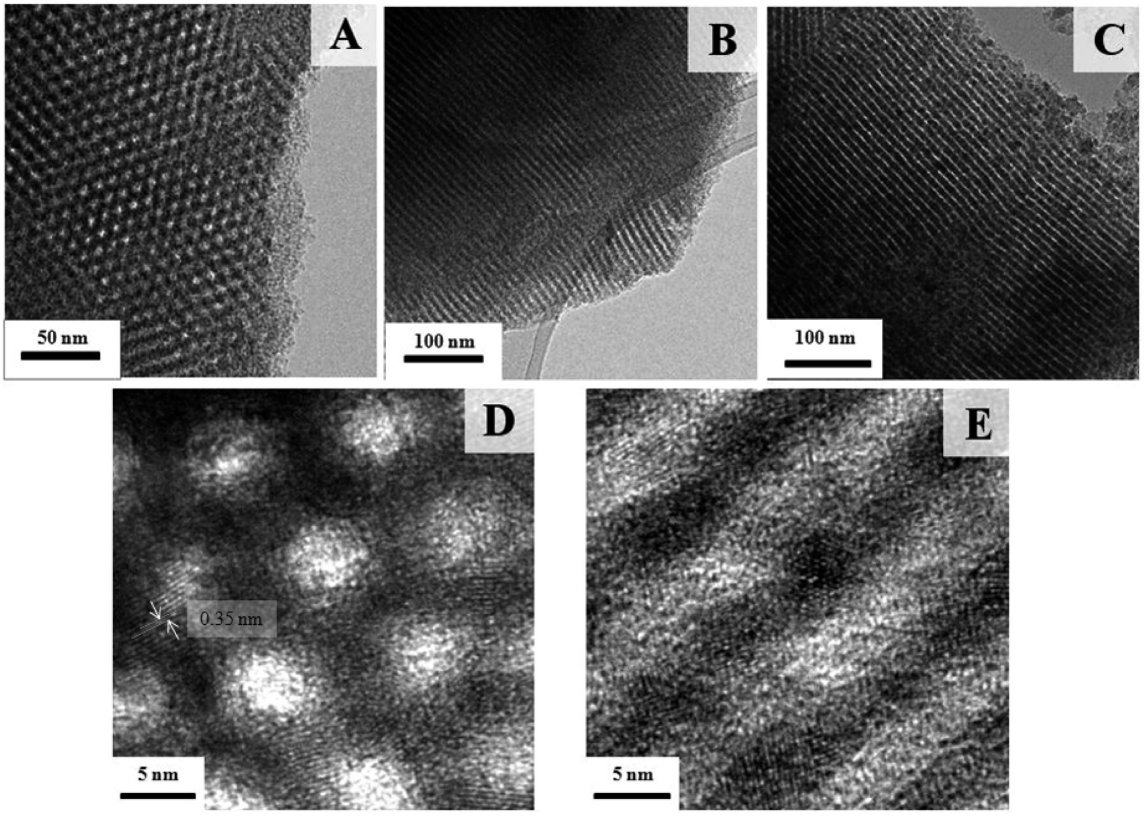

Figure 5. TEM images of the mesoporous 65Ti-35C composites calcined at (a, b) 450 and (c−e) 600 °C in N_2, view from the (b, c, and e) [110] and (a, d) [001] directions.

800 °C, whereas the calcination of TiO_2 and carbon bulks at 1000 °C generate the Magneli phases of titanium oxide (Ti_nO_{2n-1}) and TiC. It is noted that the titanium oxycarbide (TiOC) phases could be generated before the formation of titanium carbide at high temperature.[17b] In addition, the wide-angle XRD patterns of these two compounds are undistinguished, which means that the TiC nanocrystals may coexist with TiOC phases during carbothermal reduction at 1000 °C. Therefore, it is concluded that the reduction of titania in mesoporous 75Ti-25C and 65Ti-35C composites follows the sequence TiO_2 (anatase) → TiO_2 (rutile) → Ti_4O_7 → TiC, whereas the reaction for the composite 50Ti-50C is TiO_2 (anatase) → TiC, and no rutile and reduction to Magneli phase of Ti_4O_7 are observed, which are in good agreement with other studies.[16,18]

$$TiO_2 + xC \rightarrow TiO_{2-x} + xCO \quad (2)$$

$$nTiO_{2-x} + (1-nx)C \rightarrow Ti_nO_{2n-1} + (1-nx)CO \quad (\text{with } 4 \le n \le 9) \quad (3)$$

$$4TiO_{2-x} + (1-4x)C \rightarrow Ti_4O_7 + (1-4x)CO \quad (4)$$

$$4TiO_2 + C \rightarrow Ti_4O_7 + CO \quad (5)$$

$$Ti_4O_7 + 11C \rightarrow 4TiC + 7CO \quad (6)$$

$$TiO_2 + 3C \rightarrow TiC + 2CO \quad (7)$$

To understand the thermal properties of the mesoporous Ti−C composites, we employed TGA and DTG/DTA to determine the changes in weight loss and heat flow, respectively (Figure 4). A slight weight loss appears at 100−200 °C for all the as-made products, resulting from the water desorption and polymerization of phenol resins in the mesoporous Ti−C composites. The sharp DTG peaks occur at 300−400 °C with a significant weight loss of 53−56 wt %, which is mainly attributed to the removal of triblock copolymer. The weight losses of 10.8 and 15.7 wt % for the mesoporous composites 75Ti-25C and 65Ti-35C, respectively, are also observed when the temperature increases to 1000 °C, which is consistent with the phenomena of polymerization, dehydrogenation and carbonization of phenolic resins and carbothermal reduction of TiO_2.[8,9] It is noted that two broad weight loss peaks at 500−600 and 950−1100 °C for the mesoporous 50Ti-50C composite are observed. From the wide-angle XRD patterns, these two peaks may be attributed to the dehydrogenation and carbonization of phenolic resins and carbothermal reduction of TiO_2, respectively. In addition, the weight percentages of 50Ti-50C decreased from 31.6 wt % at 800 °C to 17.9 wt % at 1050 °C. This decreased ratio is similar to the expected value of mass change from TiO_2 to TiC (TiO_2 + 3C → TiC + 2 CO), which means that the mass loss during formation of TiC (> 1000 °C) is in good agreement with the expected value.

Figure 5 shows the TEM images of the mesoporous 65Ti-35C composites calcined at 450 and 600 °C. Large domains of highly ordered stripe-like 1D channels are clearly

observed (Figure 5a−c). It should be noted that a partial distortion of mesostructure in some domains is observed after calcined at 600 °C (Figure 5c), which can explain the phenomenon of the decrease in the scattering intensity of mesoporous 35C-65Ti composites after calcination at 600 °C (Figure 1). TEM images clearly show that the anatase nanocrystals are embedded into the ordered mesoporous carbon frameworks, resulting in the formation of "reinforced-concrete"-like structure (Figure 5d,e). The lattice fringe can be clearly measured in TEM images with average *d*-spacing of 0.35 nm when calcined at 600 °C, which is in good agreement with the (101) reflection of anatase (d_{101}) from the corresponding wide-angle XRD pattern.

The molecular structure change in graphitization degree of Ti−C composites was examined by X-ray absorption spectroscopy (XAS). In addition, the Ti *K*-edge XANES was used to derive information on the coordination environment of Ti atoms in Ti−C composites. The XAS spectra (Figure 6a) of the mesoporous 65Ti-35C composite show a sharp 1s → π^* peak at 285.1 eV and the 1s → σ^* edge at near 292 eV, which correspond to fingerprints of sp^2- and sp^3-bonded carbons in 65Ti-35C composite, respectively.[20] The feature at 288 eV originally assigned to interlayer bands with σ symmetry is contributed from the C−H σ^* band and related to the presence of hydrogen after incomplete pyrolysis of the hydrocarbon precursors.[20,21] The sharp band at 288 eV associated with C−H σ^* bonds diminishes apparently after calcination at 450 °C, which is contributed from the decomposition of the triblock copolymer. The intensity ratio of the 1s → π^* to C−H σ^* bands for the mesoporous 65Ti-35C composites increases upon increasing calcination temperature (above 450 °C), indicating that the increase in sp^2 bonds is mainly due to the clean surface and the possible break in surface molecular bonds.[21] The relative heights of the 1s → π^* and 1s → σ^* featured at 285.1 and 292 eV, respectively, can be used to represent the sp^2- and sp^3-bonded carbon contents, and the 1s → π^*/1s → σ^* ratios at various temperatures from 450 to 1000 °C increased from 0.07 to 1.05, clearly demonstrating the increase in graphitization. After calcination at 450−800 °C, the shoulder at 284.1 eV for the sp^2 matrix can be observed. Analogously, the shoulder derived from the 1s → π^* preedge region can be ascribed to distorted sp^2 bonds (π'^*).[20] In addition, the distorted sp^2 bonds diminish at high temperature, depicting the high rigidity of ordered mesostructures after calcination. However, the shoulder peak remains in the spectrum of the Ti−C composites at 800 °C, highlighting the residual disordered phase surviving. Several studies have used carbon K-edge of highly oriented pyrolytic graphite (HOPG) to explain the XAS results of carbon-based materials.[20,22] A previous study investigated the XAS spectra of commercial TiC powders at various temperatures, and found that spectra of TiC exhibited three major peaks centered at ~285.4, ~288.5, and ~291.8 eV.[22] The sp^2-type bonding at 285.4 eV was dominant in commercial TiC powders, which is in good agreement with the results obtained in this study.

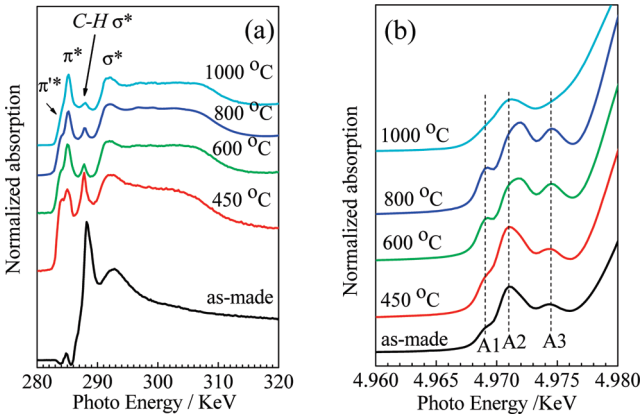

Figure 6. Normalized (a) C *K*-edge and (b) Ti *K*-edge absorption spectra of the as-made and calcined mesoporous 65Ti-35C composites. The calcination was carried out at various temperatures ranging from 450 to 1000 °C under a N_2 atmosphere.

The nature of the carbon in the mesoporous Ti−C composites was also confirmed by Raman spectroscopy. Figure S8 in the Supporting Information shows the Raman spectra of mesoporous Ti−C composites after calcination at 800 °C. The Raman spectra of mesoporous Ti−C composites show two peaks at 1319 and 1591 cm^{-1}, which correspond to the characteristics of disordered graphite (D band) and the Raman-active E_{2g} vibration mode of graphite layers with sp^2 carbon structures (G band).[23] The relative intensity ratio of G- and D-band (I_G/I_D) is indicative of the degree of graphitization. The relative intensity ratio (I_G/I_D) of Raman spectra of mesoporous Ti−C-800 composite is around 1.2, clearing indicating the higher degree of graphitization.

The Ti *K*-edge XANES spectra (Figure 6b) show three resolved pre-edge peaks (labeled A1, A2, and A3) follow by features on the higher energy part of the rising edges. The A1 peak is due to a quadrapolar 1s → 3d(t_{2g}) transition, the A2 is dipolar in nature but also includes a little quadrapolar component (1s → 3d(e_g)), whereas the A3 peak is a pure dipolar component.[24,25] In addition, the occurrence and shape of A3 peak provides a sensitive probe for the degree of distortion.[24] The Ti K-edge spectra show that the A3 peak for mesoporous Ti−C composites increases upon the increasing calcination temperatures from 450 to 800 °C. In addition, the A2 peak shifts to higher energy region, clearly showing the distortion around the TiO_6 octahedral sites, presumably because of the phase transformation from anatase to rutile.[26] At 1000 °C, only A2 peak is observed, demonstrating the

(20) (a) Larciprete, R.; Lizzit, S.; Bott, S.; Cepek, C.; Goldoni, A. *Phys. Rev. B* **2002**, *66*, 121402. (b) Shimomura, K.; Muramatsu, Y.; Denlinger, J. D.; Gullikson, E. M. *Int. J. Quantum Chem.* **2009**, *109*, 2722–2727.
(21) Abbas, M.; Wu, Z. Y.; Zhong, J.; Ibrahim, K.; Fiori, A.; Orlanducci, S.; Sessa, V.; Terranova, M. L.; Davoli, I. *Appl. Phys. Lett.* **2005**, *87*, 051923.
(22) Dash, R.; Chmiola, J.; Yushin, G.; Gogotsi, Y.; Laudisio, G.; Singer, J.; Fischer, J.; Kucheyev, S. *Carbon* **2006**, *44*, 2489–2497.
(23) Ferrari, A. C.; Robertson, J. *Phys. Rev. B* **2000**, *61*, 14095–14107.
(24) Fronzoni, G.; De Francesco, R.; Stener, M.; Causa, M. *J. Phys. Chem. B* **2006**, *110*, 9899–9907.
(25) Pickup, D. M.; Abou Neel, E. A.; Moss, R. M.; Wetherall, K. M.; Gerry, P.; Smith, M. E.; Knowles, J. C.; Newport, R. J. *J. Mater. Sci.: Mater Med.* **2008**, *19*, 1681–1685.
(26) Farges, F.; Brown, G. E.; Rehr, J. J. *Phys. Rev. B* **1997**, *56*, 1809–1819.

Scheme 1. Formation of Highly Ordered 2D Hexagonal Mesoporous Ti−C Composites via Supramolecular Self-Assembly and In situ Crystallization

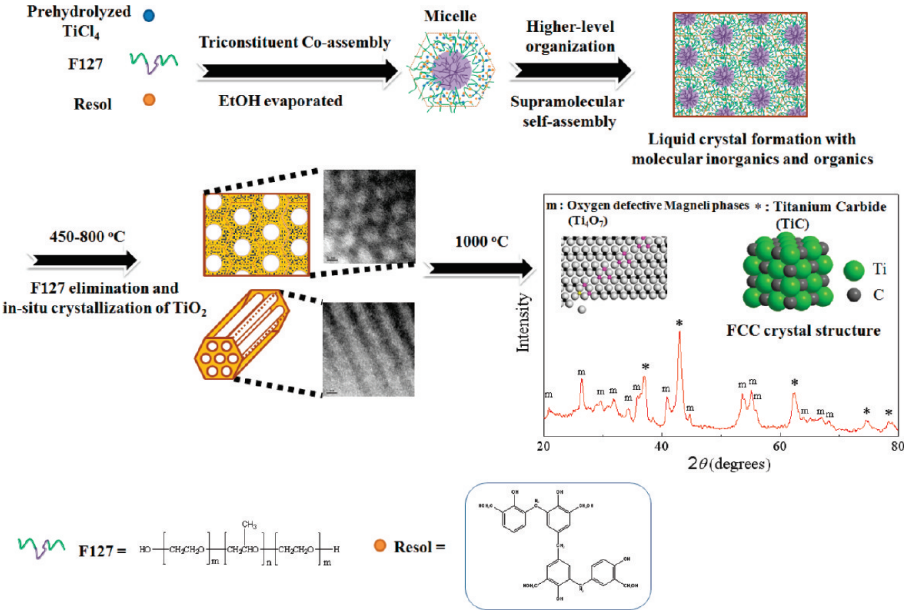

formation of low distorted octahedrons with 6-fold coordinated titanium (TiC). This result is also in good agreement with the results obtained from wide-angle XRD patterns and TGA analysis.

In this study, a series of highly ordered 2D hexagonal mesoporous Ti−C composites with various C/Ti mass ratios are synthesized via supramolecular self-assembly and in situ crystallization. Scheme 1 shows the proposed formation of mesoporous Ti−C composites with various carbon contents after calcination at different temperatures. The soluble resol, prehydrolyzed $TiCl_4$, and triblock copolymer F127 were used as the carbon source, inorganic precursor, and SDA, respectively. The dissolution of $TiCl_4$ in H_2O/EtOH solution is a violently exothermic reaction and generates HCl, resulting in production of strong acid solution ($[H^+] > 1$ mol L^{-1}), and collection of chloro-hydroxy-alkoxide $[Ti(OH)_2(H_2O)_n(Z)_x]^{(2-x)+}$ (Z = OH, Cl, OEt; $x < 2$) species.[27] The generation of HCl avoids the aggregation and condensation of TiO species. The protonation of phenol hydroxy groups of the resols can restrict the transesterification between the prehydrolyzed $TiCl_4$ and the phenol hydroxyl group.[11a] The final materials have an interpenetrating framework with "reinforced-concrete"-like structure, in which both "reinforcing-steel-bar" titania and "concrete" carbons can assembly with F127 to form mesostructure.[8,11] Large size polymer frameworks interpenetrate with titania networks during thermal polymerization of resols at 100 °C inside the mesostructure.

Conclusions

In this study, a series of highly ordered 2D hexagonal mesoporous Ti−C composites with various Ti/C mass ratios has been synthesized via supramolecular self-assembly and in situ crystallization. The mesostructured carbon is distorted by the growth of TiO_2 nanocrystals at 450−800 °C. The calcination temperatures and carbon contents have significant effect on the transformation of TiO_2 nanocrystals from anatase to rutile and then to Magneli phases and TiC. In addition, the degree of graphitization, determining by sp^2/sp^3 ratios from C *K*-edge XAS spectra, increases upon increasing calcination temperature. To the best of our knowledge, this is the first report on the phase evolution of titanium-based materials in the presence of carbon matrices with in situ carbothermal reduction and on XAS analysis of fine structures of highly ordered mesoporous titanium oxides and carbide/carbon composites. The ordered mesoporous titanium oxides and carbide/carbon composites with well-defined microstructures and specific physicochemical properties could have many potential applications in catalysis, adsorption, Li-ion battery, and supercapacitors. It can open an avenue to the design and synthesis of a multitude of cooperatively functional organic−inorganic materials, such as ordered mesoporous metals (Pt, Pd, and Sn) or metal oxides (ZnO, ZrO_2, SnO_2)-carbon composites with attractive optical, chemical, biochemical, and mechanical properties.

Acknowledgment. The authors thank the National Science Council, Taiwan, for financial supports under Grant No. NSC96-2113-M-007-027-MY3 and NSC98-2627-M-007-005. D.Y.Z. thanks the NSFC for support.

Supporting Information Available: The TGA curve of Ti−C composites in air; BET and pore size distribution; SAXS and wide-angle XRD patterns of Ti−C composites; micropore size distribution; Raman spectra (PDF). This material is available free of charge via the Internet at http://pubs.acs.org.

(27) Brinker, C. J.; Scherer, G. W. *Sol−Gel Science*; Academic Press: San Diego, 1990; pp 21−59.